INSTITUTE OF PHYSICS PUBLISHING PHYSICS IN MEDICINE AND BIOLOGY

Phys. Med. Biol. **49** (2004) 5011–5028 PII: S0031-9155(04)83247-0

An advanced boundary element method (BEM) implementation for the forward problem of electromagnetic source imaging

Zeynep Akalın-Acar and Nevzat G Gençer

Department of Electrical and Electronics Engineering, Middle East Technical University, Brain Research Laboratory, 06531 Ankara, Turkey

E-mail: ngencer@metu.edu.tr

Received 8 July 2004
Published 15 October 2004
Online at stacks.iop.org/PMB/49/5011
doi:10.1088/0031-9155/49/21/012

Abstract

The forward problem of electromagnetic source imaging has two components: a numerical model to solve the related integral equations and a model of the head geometry. This study is on the boundary element method (BEM) implementation for numerical solutions and realistic head modelling. The use of second-order (quadratic) isoparametric elements and the recursive integration technique increase the accuracy in the solutions. Two new formulations are developed for the calculation of the transfer matrices to obtain the potential and magnetic field patterns using realistic head models. The formulations incorporate the use of the isolated problem approach for increased accuracy in solutions. If a personal computer is used for computations, each transfer matrix is calculated in 2.2 h. After this pre-computation period, solutions for arbitrary source configurations can be obtained in milliseconds for a realistic head model. A hybrid algorithm that uses snakes, morphological operations, region growing and thresholding is used for segmentation. The scalp, skull, grey matter, white matter and eyes are segmented from the multimodal magnetic resonance images and meshes for the corresponding surfaces are created. A mesh generation algorithm is developed for modelling the intersecting tissue compartments, such as eyes. To obtain more accurate results quadratic elements are used in the realistic meshes. The resultant BEM implementation provides more accurate forward problem solutions and more efficient calculations. Thus it can be the firm basis of the future inverse problem solutions.

1. Introduction

Magnetoencephalography (MEG) and electroencephalography (EEG) devices respectively measure the magnetic fields near the head and the electric potentials on the scalp surface due to the electrical activities inside the human brain. Localization of the brain activities using EEG and MEG measurements is called electromagnetic source imaging (EMSI) (Baillet *et al* 2001, Michel *et al* 2001, He 1998, Gençer *et al* 2003). The electrical activities in the brain are usually modelled using current dipoles (De Munck *et al* 1988). The purpose of EMSI is to obtain information about the spatiotemporal behaviour of these dipoles. The solution of the scalp potentials and magnetic fields for a specific dipole configuration is the *forward problem* of EMSI. Complementarily, the *inverse problem* is the localization of the sources based on the measurements and the calculations. Accurate modelling of the human head is necessary to increase the accuracy of EMSI solutions (Roth *et al* 1993, Crouzeix *et al* 1999, Huiskamp *et al* 1999). When the realistic head models are used, a numerical approach must be adopted. The most widely used numerical methods are the boundary element method (BEM) (Meijs *et al* 1989, Hämäläinen and Sarvas 1989, Cuffin 1995, Gençer and Tanzer 1999, Finke and Gulrajani 2001), the finite element method (FEM) (Thevenet *et al* 1991, Yan *et al* 1991, Haueisen *et al* 1995, Gençer and Acar 2004) and the finite difference method (FDM) (Nixon *et al* 2003, Vanrumste *et al* 2001). This study focuses on (1) increasing the accuracy of the BEM solutions with realistic head models, (2) improving the efficiency of the BEM computations and (3) generating more realistic head meshes to be used with the BEM formulations.

To increase the numerical accuracy in the solutions either the numerical formulation is improved or the quality of the meshes used in the calculations is increased. The numerical error caused by high conductivity difference between the skull and brain layer is reduced using the modified equations, as given in the isolated problem approach (IPA) (Meijs *et al* 1989, Hämäläinen and Sarvas 1989). The use of high-order elements (quadratic, cubic) in the BEM formulations (Budiman and Buchanan 1993, Gençer and Tanzer 1999, Frijns *et al* 2000) and the method of recursive integration (Frijns *et al* 2000) also increase the accuracy. While the advantages of high-order elements and recursive integration were shown by concentric spherical-shell head models they have not been applied to realistic head geometries.

When realistic head models are used, the forward problem computation time increases considerably. Usually, a pre-computation phase, such as inverting or decomposing the BEM coefficient matrix (defined in section 2) is necessary to reduce the time for the individual dipole solutions. One obvious way to reduce the computation time is to solve the potentials only at the electrode positions. Thus, a transfer matrix relating the source distribution to the potentials on the electrode locations is computed. Several researchers have exploited this idea but their approaches differed in the computation of the transfer matrix. Cuffin (1995) calculated the transfer matrix using the power series expansion of the BEM coefficient matrix. Fletcher *et al* (1995) obtained the transfer matrix by first computing the true inverse of the coefficient matrix in the BEM formulation and selecting the corresponding rows. Similarly, Fuchs *et al* (2001) computed the transfer matrix by first obtaining the LU decomposition of the coefficient matrix. Note that a method to calculate the transfer matrix for the solution of the magnetic fields at the sensor locations has not been proposed yet.

A different approach to decrease the computation time was to pre-compute the solutions over a grid of dipoles covering the brain volume. The solutions for an arbitrary source configuration are then obtained using interpolation (Ermer *et al* 2001, Yvert *et al* 2001). However, when this technique is employed, the density of grid points and the choice of

interpolation function determine the accuracy in solutions; increasing the density of grid points increases the pre-computation time.

Another important step for the forward problem solutions is to obtain numerical meshes that model the head geometry accurately. The geometry information is usually obtained from tomographic images. The meshes used for the BEM solutions model the surfaces (interfaces) between tissues of different conductivities. Usually, they represent the interfaces between the major tissues of the head, such as scalp, skull and the brain. Early studies constructed BEM meshes by triangulating manually selected points from T_1-weighted magnetic resonance (MR) images (Roth *et al* 1993, Yvert *et al* 1995). Semi-automatic segmentation of MR slices using different techniques such as region growing, thresholding and morphological operations has also been employed (Schimpf *et al* 1998, Fuchs *et al* 1998, Ermer *et al* 2001). Schimpf *et al* (1998) and Fuchs *et al* (1998) performed mesh generation by triangulating nodes placed on the surfaces of scalp, skull and brain. Note that most of the researchers in this field use T_1-weighted MR images for segmentation. However, it is difficult to isolate the skull from background and air regions using MR images, as the skull has low water content. One approach for solving this problem is to segment the skull from computed tomography (CT) images (Huiskamp *et al* 1999). Another approach is to approximate the skull layer by expanding and smoothing the brain surface (Fuchs *et al* 1998).

Recently, the inhomogeneities in the skull layer were also modelled. Oostenveld and Oostendorp (2002) compared the accuracy of the BEM and the FDM solutions for a head geometry with a hole in the skull. The effects of holes and other inhomogeneities in the skull were also investigated by Benar and Gotman (2002). Both of these studies concluded that such defects should be included in the model to improve the accuracy. However, they have not provided a general method for modelling such complex geometries.

This work contributes to the two major aspects of the forward problem solutions: the BEM implementation and the realistic head modelling. In a previous study, we have proposed the use of high-order isoparametric elements to increase the accuracy in the solutions (Gençer and Tanzer 1999). In this study, the accuracy in the BEM solutions is further improved by applying the recursive integration technique (Frijns *et al* 2000). The new BEM implementation allows the use of quadratic elements with realistic head models and is capable of handling intersecting surfaces, such as skull and eyes. To decrease the computation time, two new formulations are presented for the calculation of EEG and MEG transfer matrices that relate the sources to the fields at the sensor locations. Thus, by pre-computing the transfer matrices, forward solutions for electric and magnetic fields are reduced to simple matrix–vector multiplications. This method offers improved computational speed and lower storage requirements. IPA is also incorporated for higher accuracy. For realistic head modelling, a segmentation algorithm is developed to obtain scalp, skull, grey matter (GM), white matter (WM), eyeballs and the surrounding tissue of the eyes from multimodal (T_1-, T_2-weighted and proton density (PD)) MR images. A realistic head model is generated using quadratic isoparametric elements. Using a novel mesh generation approach, it is possible to model complex geometries such as the intersecting skull and eye boundaries.

The next section introduces the BEM and presents new formulations for calculating the transfer matrices. The segmentation and mesh generation algorithms are explained in sections 3 and 4, respectively. Finally, the results related to the segmentation and mesh generation algorithms, accuracy in the solutions and computational performance are presented.

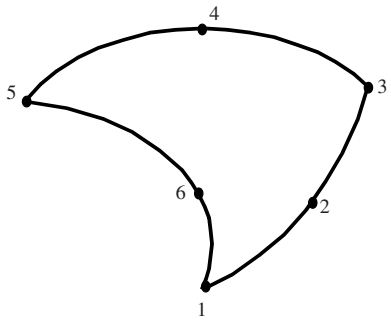

Figure 1. A 6-noded triangular, quadratic and isoparametric BEM element.

2. Boundary element method

2.1. Introduction

The electric potential ϕ and the magnetic field $\vec{B}$ due to a current dipole source $\vec{p}$ in a piecewise homogeneous volume conductor model of the head, satisfy the following integral equations (Geselowitz 1967):

$$\bar{\sigma}\phi(\vec{r}) = g(\vec{r}) + \frac{1}{4\pi}\sum_{k=1}^{L}\left(\sigma_k^- - \sigma_k^+\right)\int_{S_k}\phi(\vec{r}')\frac{\vec{R}}{R^3}\cdot \mathrm{d}\vec{S}_k(\vec{r}'), \tag{1}$$

$$\vec{B}(\vec{r}) = \vec{B}_0(\vec{r}) + \frac{\mu_0}{4\pi}\sum_{k=1}^{L}\left(\sigma_k^- - \sigma_k^+\right)\int_{S_k}\phi(\vec{r}')\frac{\vec{R}}{R^3}\times \mathrm{d}\vec{S}_k(\vec{r}'). \tag{2}$$

Here, the surfaces between different conductivity regions are denoted by $S_k, k = 1, \ldots, L$. The inner and outer conductivities of S_k are represented by σ_k^- and σ_k^+, respectively. $\vec{R} = \vec{r} - \vec{r}'$ is the vector between the field point $\vec{r}$ and the source point $\vec{r}'$, R is the magnitude of $\vec{R}$, and $\bar{\sigma}$ is the mean conductivity at the field point. The contribution of the primary sources g and $\vec{B}_0$ is defined as follows,

$$g(\vec{r}) = \frac{1}{4\pi\sigma_0}\frac{\vec{p}\cdot\vec{R}}{R^3}, \tag{3}$$

$$\vec{B}_0(\vec{r}) = \frac{\mu_0}{4\pi}\frac{\vec{p}\times\vec{R}}{R^3}, \tag{4}$$

where σ_0 is the unit conductivity and μ_0 is the permeability of the free space. The second terms in (1) and (2) are the secondary fields representing the effects of conductivity interfaces. These equations can be solved numerically by discretizing the surfaces into elements and computing the surface integrals over these elements (Barr *et al* 1966, Barnard *et al* 1967a, 1967b, Geselowitz 1967). The BEM elements used in this study are triangular, quadratic and isoparametric (figure 1). Since the elements are isoparametric, both the geometry and potentials over an element can be expressed using the same interpolation (shape) functions (Gençer and Tanzer 1999). Discretizing (1) over all elements, a set of equations with N unknowns are obtained where N is the number of nodes in the BEM mesh. In matrix notation, this can be expressed as

$$\Phi = \mathbf{g} + \mathbf{C}\Phi \tag{5}$$

where Φ is an $N \times 1$ vector of node potentials, $\mathbf{C}$ is an $N \times N$ matrix whose elements are determined by the geometry and electrical conductivity of the head and $\mathbf{g}$ is an $N \times 1$ vector representing the contribution of the primary sources. If $\mathbf{I}$ denotes the $N \times N$ identity matrix and $\mathbf{A}$ represents $\mathbf{I} - \mathbf{C}$ then

$$\Phi = \mathbf{A}^{-1}\mathbf{g}. \tag{6}$$

To eliminate the singularity in $\mathbf{A}$, the method of matrix deflation is employed (Lynn and Timlake 1968). IPA is implemented to overcome numerical errors caused by high conductivity difference around the skull layer (Hämäläinen and Sarvas 1989). Once Φ is computed, $\vec{B}$ is calculated from the potential values using (2). This can be written in matrix notation as follows:

$$\mathbf{B} = \mathbf{B}_0 + \mathbf{H}\Phi. \tag{7}$$

If there are n magnetic sensors, $\mathbf{B}$ is an $n \times 1$ vector representing the magnetic fields at the sensor locations, and $\mathbf{B}_0$ denotes the $n \times 1$ vector of magnetic fields at the same sensor locations for an unbounded homogeneous medium (as given in (4)). Here, $\mathbf{H}$ is an $n \times N$ coefficient matrix determined by the geometry and electrical conductivity of the head.

When the compartment surfaces are close to each other, or when the source is close to a surface (closer than the element size), numerical errors are observed. To overcome this problem, the recursive integration technique was proposed (Frijns *et al* 2000). In the recursive integration, the surface elements are divided into sub-elements and the numerical integration is performed on each sub-element. This process is repeated recursively until a subdivision criterion is met. Since the potential field is calculated at the original nodes, the size of the BEM matrix equation remains the same, but the accuracy of the surface integral is improved.

The head models used for the BEM implementations in the literature were constructed using non-intersecting layers that represent the main tissues, i.e., the scalp, skull and the brain. In these models, the eyes and the eye-holes in the skull were neglected to simplify the mesh generation and the BEM implementation. More complex head models have been studied to investigate the skull defects and holes in the skull. However, to model a skull with a hole, either a thin closed surface was used to represent the skull layer (Benar and Gotman 2002) or a different conductivity region was defined in the skull leading to infinitely thin layers between skull and hole regions (Oostenveld and Oostendorp 2002). To use a better head model in the numerical solutions, one must generate a BEM mesh that correctly defines the boundaries of different conductivity regions. A mesh generation algorithm that handles such cases will be presented in section 4.

2.2. Accelerated BEM for EEG

Equation (6) provides node potentials for all nodes of the BEM mesh. This section introduces a novel approach for computing the node potentials on a small subset of nodes corresponding to the electrode positions. This approach pre-calculates and stores relevant matrices, providing a significant decrease in the computation time for a given source configuration.

Let us assume that each electrode corresponds to a node in the BEM mesh. If m is the number of electrodes, then the electrode potentials can be written as

$$\Phi_e = \mathbf{D}\mathbf{A}^{-1}\mathbf{g} \tag{8}$$

where Φ_e is an $m \times 1$ vector of electrode potentials and $\mathbf{D}$ is an $m \times N$ sparse matrix to select m rows of $\mathbf{A}^{-1}$. Note that, if the rows of $\mathbf{A}^{-1}$ are computed and stored, then Φ_e can be calculated by a simple matrix–vector multiplication for any source vector $\mathbf{g}$. To obtain the rows of $\mathbf{A}^{-1}$ the following approach is used.

Let the *transfer matrix* $\mathbf{E}$ be defined as

$$\mathbf{E} = \mathbf{D}\mathbf{A}^{-1}. \tag{9}$$

Taking the transpose of both sides we obtain

$$\mathbf{E}^T = (\mathbf{A}^{-1})^T\mathbf{D}^T. \tag{10}$$

Using the identity $(\mathbf{A}^{-1})^T = (\mathbf{A}^T)^{-1}$, and multiplying both sides with $\mathbf{A}^T$, it is possible to obtain

$$\mathbf{A}^T\mathbf{E}^T = \mathbf{D}^T. \tag{11}$$

Thus, the ith column vector $\mathbf{e}_i$ of $\mathbf{E}^T$ can be obtained using the following equation

$$\mathbf{A}^T\mathbf{e}_i = \mathbf{d}_i \tag{12}$$

where $\mathbf{d}_i$ is the ith column of $\mathbf{D}^T$. Thus the $\mathbf{E}$ matrix (i.e., the required rows of $\mathbf{A}^{-1}$) can be computed using (12) with m different right-hand side vectors $\mathbf{d}_i$.

In this study, the accelerated BEM approach is also extended to incorporate the IPA. Let the surfaces S_1, S_2 and S_3 represent the scalp, skull and brain surfaces in a three-layer head model, respectively. Then, equation (5) can be expressed in block matrix form as follows,

$$\begin{bmatrix}\Phi_1\\ \Phi_2\\ \Phi_3\end{bmatrix} = \begin{bmatrix}\mathbf{C}_{11} & \mathbf{C}_{12} & \mathbf{C}_{13}\\ \mathbf{C}_{21} & \mathbf{C}_{22} & \mathbf{C}_{23}\\ \mathbf{C}_{31} & \mathbf{C}_{32} & \mathbf{C}_{33}\end{bmatrix}\begin{bmatrix}\Phi_1\\ \Phi_2\\ \Phi_3\end{bmatrix} + \begin{bmatrix}\mathbf{g}_1\\ \mathbf{g}_2\\ \mathbf{g}_3\end{bmatrix} \tag{13}$$

where the potentials on the corresponding surfaces are denoted by Φ_1, Φ_2 and Φ_3. The ratio of the conductivities across S_3 can be defined as $\beta = \frac{\sigma_2}{\sigma_3}$, where σ_2 and σ_3 are the conductivities of the second and the third layers, respectively. If $\beta \ll 1$, then Φ_1 and Φ_2 are much smaller than Φ_3 in magnitude causing numerical errors in matrix solutions. When IPA is applied, the source terms are modified as (Hämäläinen and Sarvas 1989)

$$\mathbf{g}' = \begin{bmatrix}\mathbf{g}'_1\\ \mathbf{g}'_2\\ \mathbf{g}'_3\end{bmatrix} = \begin{bmatrix}\beta\mathbf{g}_1\\ \beta\mathbf{g}_2\\ \beta\mathbf{g}_3 - \frac{2\sigma_2}{\sigma_2+\sigma_3}\Phi_3^0\end{bmatrix}, \tag{14}$$

and the resulting potentials can be written as

$$\Phi' = \mathbf{A}^{-1}\mathbf{g}' = \begin{bmatrix}\Phi'_1\\ \Phi'_2\\ \Phi'_3\end{bmatrix} = \begin{bmatrix}\Phi_1\\ \Phi_2\\ \Phi_3 - \Phi_3^0\end{bmatrix}. \tag{15}$$

In equations (14) and (15), Φ_3^0 is the potential on the surface S_3 when the head is represented by a homogeneous brain region (i.e., the skull and scalp layers are omitted). Φ_3^0 can be obtained from

$$\Phi_3^0 = (\mathbf{A}_s)^{-1}\,\mathbf{g}_3^0 \tag{16}$$

where $\mathbf{A}_s$ is in the form of $(\mathbf{I} - \mathbf{C}'_{33})$ and $\mathbf{g}_3^0$ is the corresponding source term. Here, the matrix $\mathbf{C}'_{33}$ is the scaled and deflated version of $\mathbf{C}_{33}$ (Hämäläinen and Sarvas 1989).

As a result, the accelerated approach for potential field calculations using IPA starts with the calculation of the transfer matrix $\mathbf{E}$ and $\mathbf{A}_s$. Once these matrices are computed and stored, the potentials due to an arbitrary source configuration can be obtained as follows: (1) Φ_3^0 is computed using (16); (2) $\mathbf{g}'$ is calculated using (14); and (3) Φ_e is solved using (8).

2.3. Accelerated BEM for MEG

An accelerated approach can also be developed to obtain magnetic fields. To calculate the magnetic field at the sensor locations from (7), the potential field at all nodes is used. However, since

$$\mathbf{H}\Phi = \mathbf{H}\mathbf{A}^{-1}\,\mathbf{g}, \tag{17}$$

equation (7) can be rewritten as

$$\mathbf{B} = \mathbf{B}_0 + \mathbf{M}\mathbf{g} \tag{18}$$

where

$$\mathbf{M} = \mathbf{H}\mathbf{A}^{-1}. \tag{19}$$

The $\mathbf{M}$ matrix is the $n \times N$ *transfer matrix* which relates the source vector $\mathbf{g}$ to the magnetic field measurements. $\mathbf{M}$ can be pre-computed using the same technique as given in equations (10) and (11). Thus, the ith column vector $\mathbf{m}_i$ of $\mathbf{M}^T$ can be obtained using the following equation,

$$\mathbf{A}^T\mathbf{m}_i = \mathbf{h}_i \tag{20}$$

where $\mathbf{h}_i$ is the ith column of $\mathbf{H}^T$. Once $\mathbf{M}$ is computed and stored, the magnetic field for an arbitrary source configuration can be solved without computing the potentials at all nodes.

This method can also be extended to be used with the IPA. When IPA is applied, the potentials are modified as follows,

$$\Phi' = \Phi - \Phi'' \tag{21}$$

where Φ and Φ' are as given in equations (13) and (15), and Φ'' is defined as

$$\Phi'' = \begin{bmatrix} 0 \\ 0 \\ \Phi_3^0 \end{bmatrix}. \tag{22}$$

Then, equation (7) can be rewritten as

$$\begin{aligned} \mathbf{B} &= \mathbf{B}_0 + \mathbf{H}(\Phi' + \Phi'') \\ &= \mathbf{B}_0 + \mathbf{H}\Phi' + \mathbf{H}\Phi'' \\ &= \mathbf{B}_0 + \mathbf{H}\mathbf{A}^{-1}\,\mathbf{g}' + \mathbf{H}\Phi''. \end{aligned} \tag{23}$$

Since Φ'' is zero for the first and the second layers we can write $\mathbf{H}\Phi''$ as

$$\mathbf{H}\Phi'' = [\mathbf{H}_1\ \mathbf{H}_2\ \mathbf{H}_3] \begin{bmatrix} 0 \\ 0 \\ \Phi_3^0 \end{bmatrix} = \mathbf{H}_3\Phi_3^0. \tag{24}$$

Therefore, equation (23) becomes

$$\mathbf{B} = \mathbf{B}_0 + \mathbf{M}\mathbf{g}' + \mathbf{H}_3\Phi_3^0. \tag{25}$$

As a result, to obtain fast magnetic field solutions, first the matrices $\mathbf{M}, \mathbf{H}_3$ and $\mathbf{A}_s^{-1}$ are computed and stored. After this pre-computation stage, the solutions for arbitrary source configurations can be obtained using (25) with simple matrix–vector multiplications.

3. Segmentation

To create a realistic head model, one must first classify the main tissues of the head from high resolution volume images. Segmentation is the process of classifying image elements that have the same properties. There are three major segmentation methods in the literature: (1) the deterministic methods that use classical image processing tools like thresholding, region growing and morphological operations (Brummer *et al* 1993, Atkins and Mackiewich 1998, Tang *et al* 2000, Shan *et al* 2002); (2) the statistical methods based on probabilistic methods that may also estimate the inhomogeneity in the MR images (Wells *et al* 1994, Held *et al* 1997, Joshi *et al* 1999); and (3) methods that use a deformable atlas (Sandor and Leahy 1997, Hartmann *et al* 1999).

To use realistic head models, in general, only the main tissues in the head, such as scalp, skull and brain layers, are included (Roth *et al* 1993, Fuchs *et al* 1998, Yvert *et al* 1995, Kristeva-Feige *et al* 1997, Schimpf *et al* 1998, Huiskamp *et al* 1999, Crouzeix *et al* 1999, Rao *et al* 2000, Van't Ent *et al* 2001, Ermer *et al* 2001, Wang and Gotman 2001, Cuffin *et al* 2001). To classify these tissues, usually, T_1-weighted MR images are employed, since it provides high soft tissue contrast. If cerebrospinal fluid (CSF) is to be included in the model, T_1-weighted images are not sufficient since CSF cannot be distinguished from the skull.

In this work, the scalp, skull, CSF, eyes, GM and WM are segmented from the three-dimensional multimodal MR images of the head. A hybrid algorithm is developed that applies the snakes algorithm, region growing, thresholding and morphological operations (Akalın and Gençer 2000). The segmentation process begins by removing the background from the volume data. For this purpose, first a threshold is selected using the whole head PD images. The threshold is found automatically using Nobuyuki's method (Nobuyuki 1979). After obtaining the threshold for the background, the snakes algorithm (Kass *et al* 1987) with the gradient vector flow (Xu and Prince 1998) is applied to each slice. The snakes algorithm is used to obtain the scalp as a closed surface. After removing the background, the skull and sinus regions are extracted from each PD image using thresholding (note that it is not possible to distinguish the skull and sinus regions from the multimodal MR data). To simplify the segmentation of scalp, a raw image of the cortical surface is obtained from the T_1-weighted images using thresholding and region growing. To identify the eye tissues (i.e., the eyeballs, fat and muscle tissues connected to the rear surface of the eyeballs) an eye template is obtained from a T_1-weighted slice where the eyes have the largest cross-section. The use of this template confines the region over which the region growing algorithm is applied at each slice. Using this template, the fat and muscle tissues are segmented from the T_1-weighted images. The eyeballs are then extracted from the T_2-weighted images. The scalp is segmented from the unlabelled voxels using the thresholding, region growing and morphological operations. When the segmented regions are removed from the images, the remaining regions include the CSF, WM and GM. To determine the CSF–GM and the GM–WM boundaries two thresholds are chosen from the T_1-weighted images. After thresholding, the GM and WM are obtained by region growing. The remaining voxels are then labelled according to their neighbours.

4. Mesh generation

The BEM uses a surface mesh that defines the conductivity boundaries. This mesh can be obtained from the segmented tissue boundaries using the triangulation algorithms, such as Marching Cubes (Lorensen and Cline 1987) and Adaptive Skeleton Climbing (ASC) (Poston *et al* 1998). In the previous EMSI studies, the meshes are generated by (1) first placing equally distributed nodes on the tissue boundaries and then triangulating these nodes

(Fuchs *et al* 1998, Schimpf *et al* 1998); (2) meshing the contour points of the layers at consecutive slices (Yvert *et al* 1995, Crouzeix *et al* 1999, Roth *et al* 1993, Rao *et al* 2000); (3) using free (Ermer *et al* 2001) or commercial software packages (Van't Ent *et al* 2001, Wang and Gotman 2001, Huiskamp *et al* 1999). In all these models, the first-order (linear) elements are used and the tissues are assumed to be non-intersecting. In this work, we used ASC, filtering and coarsening operations to obtain a mesh with linear elements. We obtained quadratic elements during a second coarsening process. To include eye tissues into the model, we generated intersecting meshes for outer-skull and eyes.

4.1. Generation of individual meshes

To obtain the mesh from segmentation data, first the ASC algorithm is used for triangulation. This algorithm places one or more triangles in each boundary voxel. The triangulated surface is then smoothed using a surface signal low-pass filter algorithm (Taubin 1995). Thus, the high frequencies caused by noise and the slice effect of the MR images are suppressed. During the smoothing process, the vertices of the triangulated surface are moved but the connectivity of the faces remains unchanged. The number of triangles is reduced using a coarsening algorithm based on iterative edge contraction and quadric error metrics (Heckbert and Garland 1999). At every step of coarsening, the neighbour nodes with lowest errors are connected together and a coarse mesh is obtained. The resulting mesh may contain some undesirable topological artefacts, such as disconnected or multiply connected components and singular nodes. These artefacts are corrected to create a single manifold surface that represents the given boundary (Guziec *et al* 2001).

To obtain a coarse mesh with second-order elements from a dense mesh with first-order elements, a modified coarsening process is applied. For this purpose, additional nodes are generated at the edges of each first-order element. The modified coarsening algorithm takes these additional nodes into account and fits them to the original surface defined by the dense mesh. When the common edge of the two elements contracts (i.e., an edge becomes a node), the middle nodes of the neighbouring elements are moved to fit the original surface. As a result, the element groups of the fine mesh are represented by a smaller number of quadratic elements.

In the head geometry, where the CSF is very thin, the cortex and the skull may touch each other. Thus, those regions may intersect during the mesh generation. Such regions are automatically detected and the corresponding nodes are perturbed in their normal directions to prevent intersections.

4.2. Mesh generation for intersecting surfaces

In the previous BEM studies, the boundaries have been represented as closed, non-intersecting surfaces. However, in the actual head, this is not always the case (for example, eyes, tumours, implanted plaques, etc). In this section, the mesh generation approach for intersecting surfaces will be explained for eye tissues.

When the eyes are to be included in the model, the skull–scalp interface can no longer be assumed as a closed surface. In such a case, there are skull–eye, skull–scalp and eye–scalp interfaces. In this study, the outer and inner surfaces of the skull are obtained (using the snakes algorithm) as closed surfaces from the segmented image data. Meshes are then created for the inner and outer surfaces of the skull, and for the two eyes, separately. An automatic algorithm is applied to the intersecting surfaces of the outer-skull and eyes to form a single mesh of skull and eyes (Lo 1995).

The mesh generation algorithm for intersecting surfaces can be summarized as follows: (1) find the intersections between the surfaces of skull and one eye, (2) determine a closed loop from the intersection of the line segments, (3) remove all the triangular elements of the intersection loop, (4) generate intermediate nodes along the intersection loop, (5) identify disjointed patches of the triangular elements, (6) remove the elements of the skull that remain in the eye region, (7) generate new elements using advancing front technique (Lohner and Parikh 1988) by selectively picking individual surface parts. To obtain the mesh of the skull and eyes, first one eye is intersected with the skull, and then the other eye is intersected with the previously obtained skull–eye mesh.

5. Results

5.1. Accuracy and efficiency of the BEM

5.1.1. Increasing accuracy using the recursive integration. The BEM formulation used in this work was previously used to test the accuracy for a concentric three-spheres model (Gençer and Tanzer 1999). The radii of the spheres were 10, 9 and 8 cm with conductivities 0.2, 0.005 and 0.2 S m^{-1}, respectively. The analytical and numerical solutions were compared using the relative difference measure (RDM) (Meijs *et al* 1989). For a specific mesh with second-order elements, the computed RDMs were found to be less than 2% for both potential and magnetic field solutions. However, it is observed that, as the conductivity ratio between the skull and the brain (β) decreases and/or the layers get close to each other, the numerical error in the solutions increases. To assess the numerical method for such a case, the three-layer spherical Rush and Driscoll model (Rush and Driscoll 1969) is used. In this model, the radii of the spheres are 9.2, 8.5 and 8 cm, and the conductivities are 0.2, 0.0025 and 0.2 S m^{-1}, respectively. Thus the thickness of the inner layer and β for this model are smaller compared to the three-spheres model used in the previous study (Gençer and Tanzer 1999).

The BEM mesh used in the simulations has 512 elements and 1026 nodes per layer. Note that this yields element edge sizes larger than the skull thickness, thus numerical errors must be expected. Using this mesh, the previous BEM implementation generates RDMs of the order of 20–30% for tangential dipoles located on the z-axis. The maximum error occurs when the dipole is located 2 mm below the skull layer. To improve the accuracy in solutions, the recursive integration technique is employed (Frijns *et al* 2000). When one-step recursive integration is applied, the maximum RDM decreases to 2.2%. The RDMs slightly decrease for further iterations. Since the effect of the secondary magnetic fields is low in the concentric spheres model, the change in the magnetic field due to recursive integration is less than 1%.

5.1.2. Computation times. After segmentation and mesh generation processes, the BEM implementation of the forward problem requires a number of processing stages. To illustrate the computation load of each stage the computation times are recorded for a specific head model and electrode/sensor configuration (256 electrodes/sensors). The head model includes four different tissue types: the eyes, scalp, skull and the brain. The corresponding BEM mesh has 7988 nodes and 4026 quadratic elements. The solutions are obtained using a nonoptimized iterative solver (biconjugate gradient method). For computations, a 2.4 GHz Pentium IV personal computer (PC) with 1 GB memory is used. The BEM implementation is written using C++ programming language. Table 1 shows the computation times at various stages.

Table 1. Computational complexity for a realistic mesh with 7988 nodes; A_s matrix has 1910 nodes.

Matrix filling (**A** matrix)	8 min
Single solution ($\mathbf{A}\Phi = \mathbf{g}$)	2 min
Calculation of **E** (256 electrodes)	2.2 h
Matrix filling ($\mathbf{A}_s$ matrix)	0.6 min
Calculation of $\mathbf{A}_s^{-1}$ matrix	20 s
Matrix filling (**H** matrix)	22 s
Calculation of **M** (256 sensors)	2.2 h
Calculation of the modified right-hand side (RHS)	10 ms
Calculation of the electrode potentials using **E**	102 ms
Calculation of the sensor fields using **M**	137 ms

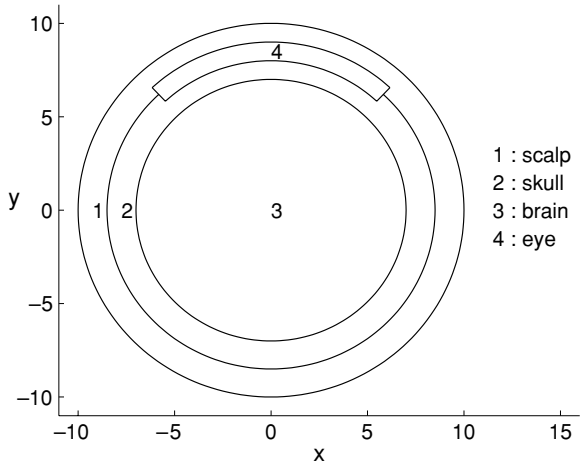

Figure 2. The cross-section of the model used in the FEM and BEM calculations. Regions corresponding to scalp, skull, brain and eye are labelled as 1, 2, 3 and 4, respectively.

5.2. Validation of the intersecting meshes

The BEM implementation that uses intersecting meshes is tested using the model shown in figure 2. The model is based on the concentric three-spheres model with an additional inhomogeneity intersecting the outer-skull layer to model a single eye. Since an analytical solution is not possible for such a head geometry, the numerical solutions are compared with the results obtained by FEM (Özdemir and Gençer 1997, Acar and Gençer 1999, Gençer *et al* 2003).

For comparison, first a FEM mesh is constructed and the elements that are on the conductivity boundaries in the FEM model are used to create the BEM mesh. The RDMs are calculated for nine dipoles located radially and tangentially at different depths. The tests are performed for five cases assigning different conductivity values to the scalp, skull, brain and eye (table 2). In the first case, the model is assumed to be homogeneous, in the second case the conductivity of the brain is increased to compare the BEM and FEM solutions. The results of the two cases are also compared with the analytical solutions and the RDMs are found to be less than 1%. In the third case, the tissue conductivities surrounding the eye (region 4) are changed. The scalp conductivity is increased and the skull conductivity is decreased. In the fourth case, all tissue conductivities are the same but the eye conductivity is increased.

Table 2. Conductivities (in S m^{-1}) of the tissues in figure 2 for five different cases.

	Scalp (1)	Skull (2)	Brain (3)	Eye (4)
Case 1	0.2	0.2	0.2	0.2
Case 2	0.2	0.2	0.4	0.2
Case 3	0.3	0.1	0.2	0.2
Case 4	0.2	0.2	0.2	0.5
Case 5	0.2	0.005	0.2	0.5

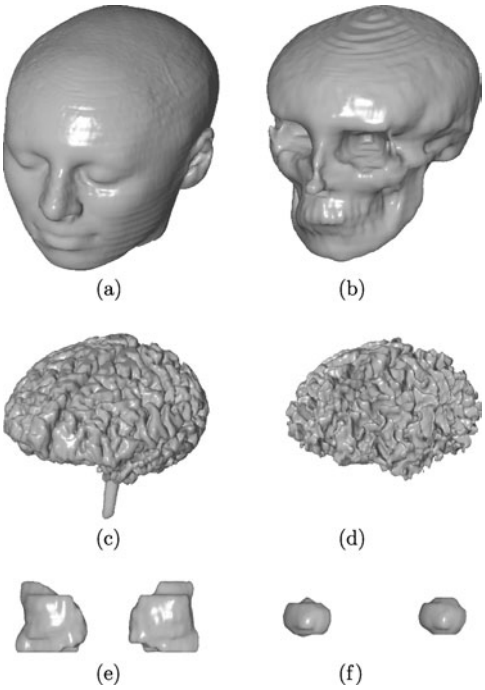

Figure 3. Segmented tissues of the whole head (a) scalp, (b) skull, (c) cortex, (d) WM, (e) eyes and (f) eyeballs.

For the last case, realistic conductivities are assigned to the tissues. We observed that the RDMs between the potential fields of the FEM and BEM models are below 1% for all cases, validating the BEM implementation for intersecting surfaces.

5.3. Segmentation

The segmentation procedure explained in section 3 was developed using the simulated MR images downloaded from the BrainWeb (Cocosco *et al* 1997). Once the algorithm becomes capable of identifying the basic features of the head from the simulated images, it is applied to real multimodal MR images. The images were acquired axially using a 1.5 T magnet. The corresponding MR sequence parameters are as follows: TR = 540 ms, TE = 12 ms for T_1-weighted images, TR = 3140 ms, TE = 24.9 ms for T_2-weighted images, and TR = 3140 ms, TE = 87 ms for PD images. All three images were acquired on a single run which ends the need to co-register the images. 12 bit, 256 × 256 pixel images corresponding to 72 slices of 3 mm thickness are processed. The segmented scalp, skull, cortex, WM, eyes and eyeballs are presented in figure 3.

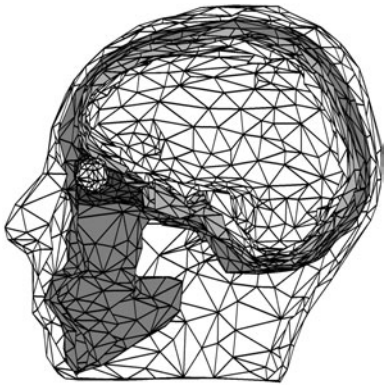

Figure 4. Cut-away view of the BEM mesh showing the inner layers. For simplicity in illustrations the quadratic elements of the mesh are displayed as linear elements.

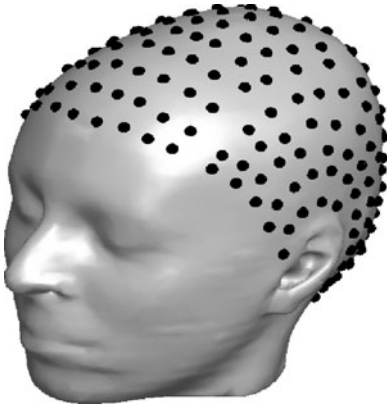

Figure 5. The locations of the 256 electrodes on the scalp surface.

5.4. Mesh generation

The mesh generation algorithm that uses triangulation, smoothing, and coarsening operations is applied to the segmented volumes of scalp, skull, cortex, eyes and eyeballs. The algorithm described in section 4.2 is applied for the intersecting surfaces of the eyeballs and skull layers. Figure 4 shows the cut-away view of the BEM mesh that models eyes, scalp, skull, CSF and brain. The mesh contains 9906 nodes and 4984 elements.

5.5. Sensitivity of measurements to eye conductivity

To investigate the effects of eyes on the forward problem solutions we compared the potential and magnetic field solutions for varying eye conductivities (Akalın and Gençer 2002). The head model includes four tissues: scalp, skull, brain and eyes. A 256-electrode Neuroscan cap is used to obtain realistic electrode positions on the scalp surface. The electrode positions are registered using a Polhemus/Fastrak digitizer (figure 5).

The calculations are performed for a single dipole located at varying distances and orientations with respect to an eye surface. The eye conductivity is assumed to be 0.5 S m^{-1}. The RDMs and RDM*s (Meijs *et al* 1989) are calculated between the two models: a realistic

Table 3. Effect of eyes on the potential solutions. The potentials using the two head models are compared. One of the head models does not include the eyes. RDMs and RDM*s for a dipole located 1.5 cm away from the eye surface are presented. The dipole is oriented tangentially and perpendicularly to the eye.

Dipole orientation	RDM (%)	RDM* (%)
Tangential	3.58	2.42
Perpendicular	6.07	4.97

model with eyes and without eyes. The results obtained for the potential solutions, for a dipole located 1.5 cm away from an eye surface, are summarized in table 3. It is observed that as the dipole approaches the eye surface the effects of eyes become significant for the potential solutions. Thus we suggest including the eyes in the numerical model especially for sources in the pre-frontal lobe. For the magnetic field calculations, the RDMs for all dipole locations and configurations are found to be less than 0.1%.

6. Conclusions and discussion

This study describes a fast and accurate BEM implementation and a novel approach for creating detailed realistic BEM models from the multimodal MR images. The implementation uses second-order isoparametric elements, and applies the IPA and recursive integration techniques for improved accuracy.

The accuracy of the original BEM formulation (Gençer and Tanzer 1999) was improved by using the recursive integration technique and tested using the Rush and Driscoll head model. For a specific head model of 512 elements and 1026 nodes on each surface, the maximum RDM decreases to 2.2% for a dipole located 2 mm apart from the skull.

Two new formulations were developed to compute the transfer matrices of EEG and MEG. The formulations allow the use of the IPA with the corresponding transfer matrices. The formulation presented in sections 2.2 and 2.3 assumes a three-layer realistically shaped head model. Thus, it is not applicable for an inhomogeneous brain region. In fact, a more general formulation must be derived to apply the IPA when there are inhomogeneities inside the skull, such as cerebrospinal fluid, white matter, grey matter or a large ventricle.

The computation times of the transfer matrices are 2.4 h when a PC (Pentium IV, 2.4 MHz) and a nonoptimized iterative solver (biconjugate gradient method) are used for calculations. Note that this can be further reduced by using better iterative algorithms, pre-conditioning, and optimized solvers. Once these matrices are calculated, the forward problem solutions for a realistic head model can be obtained using simple matrix multiplications in milliseconds.

In this study, we have focused on the computation of the MEG transfer matrix for a fixed head/helmet configuration. The transfer matrix method that we have proposed is computationally efficient compared to the conventional approach (where the potential of all nodes is calculated). This is especially evident for the inverse problem solutions that require large numbers of forward problem calculations.

If the head movements are to be taken into account, corresponding sensor positions must be recorded appropriately (De Munck *et al* 2001). To use this information in the inverse problem, we may propose the following two approaches: (1) a different transfer matrix can be calculated for each head position, (2) a larger (parent) transfer matrix can be computed corresponding to a sensor set that covers a larger sensor area. The computation time for the first solution will be considerably longer compared to the case of single transfer matrix computation (for a fixed head/helmet configuration). However, we may expect smaller error in

the source localization. The second solution, however, can be computationally more efficient. The rows of the transfer matrix corresponding to a specific sensor set can be calculated from the parent matrix by using interpolation techniques. The advantages/disadvantages of these techniques must be further investigated by simulation studies.

This BEM implementation allows modelling of intersecting tissue boundaries. Thus it is possible to include complex geometries, such as eyes, into the model. To obtain realistic head models, a semi-automatic segmentation algorithm is developed to extract the scalp, skull, WM, GM and eye tissues from MR images. The algorithm was tested on simulated data downloaded from the BrainWeb, as well as on real MR data. It was observed that the segmentation algorithm is capable of detecting the main tissues of the head with their characteristic features. However, the segmentation algorithm needs to be further automated and validated on different individuals before being put to regular use.

A mesh generation algorithm was developed for creating meshes from the segmented volumes. The mesh generation algorithm uses triangulation, filtering, coarsening and topological correction operations to generate high quality meshes. The mesh generation algorithm has two important features: (1) the ability to create meshes for intersecting tissue boundaries, and (2) generation of realistic meshes with second-order elements. The eye tissues are included by creating a mesh that conforms to the intersecting boundaries of the outer-skull and eyes. The advantages of using high-order elements were presented previously (Gençer and Tanzer 1999). However, these elements have not been used in the realistic models as it is difficult to fit them to the complex head geometry. By integrating second-order element generation process into the coarsening algorithm it is now possible to use second-order elements in the realistic BEM models.

The realistic head model developed in this study was used to investigate the effects of eye conductivity on the forward problem solutions. Dipoles 1.5 cm apart from an eye surface caused changes in the potential pattern yielding RDMs of the order of 2–6%. Thus if surface voltages are to be used for source localization, eyes should be included in the head model. This is especially necessary when the sources are assumed in the pre-frontal cortex. Including eyes in the head model produced negligible effect in the magnetic field solutions (i.e., the RDMs were below 0.1%).

The realistic head modelling approach of this study can be used in future advanced BEM implementations to investigate the effects of other complex features, such as tumours and skull defects, in the head.

Acknowledgments

This work is supported by the Middle East Technical University Research Fund Projects AFP-2001-03-01-02 and BAP-2003-07-02-00-12. We would like to thank Dr Mehmet Çamurdanoğlu from the Bayındır Hospital, Dr Serdar Akyar and Dr Suat Fitöz from the Ankara University Medical Faculty for their help in supplying and analysing the MR images. We would like to thank Dr Can Erkin Acar, Dr Yeşim Serinağaoğlu Doğrusöz and Yoldaş Ataseven for reading the manuscript.

References

Acar C E and Gençer N G 1999 Forward problem solution of ESI using FEM and BEM with quadratic isoparametric elements *Proc. IEEE EMBS Conf.*

Akalın Z and Gençer N G 2000 MR kafa görüntülerinin bölütlenmesi *Biyomedikal Mühendisliği Ulusal Toplantısı Bildiriler Kitabi* **138** 138–41

Akalın Z and Gençer N G 2002 Investigating the effects of eye conductivity on EMSI forward problem using a realistic BEM head model *Proc. Int. J. Bioelectromagn.* **4** 219–20

Atkins M S and Mackiewich B T 1998 Fully automatic segmentation of the brain in MRI *IEEE Trans. Med. Imaging* **17** 98–107

Baillet S, Mosher J C and Leahy R M 2001 Electromagnetic brain mapping *IEEE Signal Process. Mag.* **18** 14–30

Barnard C L, Duck I M and Lynn M S 1967a The application of electromagnetic theory to electrocardiology: I. Derivation of the integral equations *Biophys. J.* **7** 443–62

Barnard C L, Duck I M, Lynn M S and Timlake W P 1967b The application of electromagnetic theory to electrocardiology: II. Numerical solution of the integral equations *Biophys. J.* **7** 463–91

Barr R C, Pilkington T C, Boineau J P and Spach M S 1966 Determining surface potentials from current dipoles, with application to electrocardiography *IEEE Trans. Biomed. Eng.* **13** 88–92

Benar C G and Gotman J 2002 Modeling of post-surgical brain and skull defects in the EEG inverse problem with the boundary element method *Clin. Neurophysiol.* **113** 48–56

Brummer M E, Mersereau R M, Eisner R L and Lewine R R J 1993 Automatic detection of brain contours in MRI data sets *IEEE Trans. Med. Imaging* **12** 153–66

Budiman J and Buchanan D S 1993 An alternative to the biomagnetic forward problem in a realistically shaped head model, the 'weighted vertices' *IEEE Trans. Biomed. Eng.* **40** 1048–53

Cocosco C A, Kollokian V, Kwan R K-S and Evans A C 1997 BrainWeb: online interface to a 3D MRI simulated brain database *NeuroImage Proc. 3rd Int. Conf. on Functional Mapping of the Human Brain* **5** part 2/4

Crouzeix A, Yvert B, Bertrand O and Pernier J 1999 An evaluation of dipole reconstruction accuracy with spherical and realistic head models in MEG *Clin. Neurophysiol.* **110** 2176–88

Cuffin N B 1995 A method for localizing EEG sources in realistic head models *IEEE Trans. Biomed. Eng.* **42** 68–71

Cuffin N B, Schomer D L, Ives J R and Blume H 2001 Experimental tests of EEG source localization accuracy in realistically shaped head models *Clin. Neurophysiol.* **112** 2288–92

De Munck J C, Van Dijk B W and Spekreijse H 1988 Mathematical dipoles are adequate to describe realistic generators of human brain activity *IEEE Trans. Biomed. Eng.* **35** 960–6

De Munck J C, Verbunt J P A, Van't Ent D and Van Dijk B W 2001 The use of an MEG device as 3D digitizer and motion monitoring system *Phys. Med. Biol.* **46** 2041–52

Ermer J J, Mosher J C, Baillet S and Leahy R M 2001 Rapidly recomputable EEG forward models for realistic head shapes *Phys. Med. Biol.* **46** 1265–81

Finke S and Gulrajani R M 2001 Conventional and reciprocal approaches to the forward problem of electroencephalography *Electromagetics* **21** 513–30

Fletcher D J, Amir A, Jewett D L and Fein G 1995 Improved method for computation of potentials in a realistic head shape model *IEEE Trans. Biomed. Eng.* **42** 1094–104

Frijns J H M, Snoo S L de and Schoonhoven R 2000 Improving the accuracy of the boundary element method by the use of second-order interpolation functions *IEEE Trans. Biomed. Eng.* **47** 1336–46

Fuchs M, Drenckhahn R, Wiscmann H A and Wagner M 1998 An improved boundary element method for realistic volume conductor modelling *IEEE Trans. Biomed. Eng.* **45** 980–97

Fuchs M, Wagner M and Kastner J 2001 Boundary element method volume conductor models for EEG source reconstruction *Clin. Neurophysiol.* **112** 1400–7

Gençer N G and Acar C E 2004 Sensitivity of EEG and MEG measurements to tissue conductivity *Phys. Med. Biol.* **49** 701–17

Gençer N G, Acar C E and Tanzer I O 2003 Forward problem solution of magnetic source imaging *Magnetic Source Imaging of the Human Brain* ed Z L Lu and L Kaufman (Hillsdale, NJ: Lawrence Erlbaum Associates)

Gençer N G and Tanzer I O 1999 Forward problem solution of electromagnetic source imaging using a new BEM formulation with high-order elements *Phys. Med. Biol.* **44** 2275–87

Geselowitz D B 1967 On bioelectric potentials in an inhomogeneous volume conductor *Biophys. J.* **7** 1–11

Guziec A, Taubin G, Lazarus F and Horn B 2001 Cutting and stitching: converting sets of polygons to manifold surfaces *IEEE Trans. Vis. Comput. Graphics* **7** 136–51

Hämäläinen M S and Sarvas J 1989 Realistic conductivity geometry model of the human head for interpretation of neuromagnetic data *IEEE Trans. Biomed. Eng.* **36** 165–71

Hartmann S L, Parks M H, Martin P R and Dawant B M 1999 Automatic 3-D segmentation of internal structures of the head in MR images using a combination of similarity and free-form transformations: II. Validation on severely atrophied brains *IEEE Trans. Med. Imaging* **18** 917–26

Haueisen J, Ramon C, Czapski P and Eiselt M 1995 On the influence of volume currents and extended sources on neuromagnetic fields: a simulation study *Ann. Biomed. Eng.* **23** 728–39

He B 1998 High-resolution source imaging of brain electrical activity *IEEE Eng. Med. Biol.* **17** 123–9

Heckbert P S and Garland M 1999 Optimal triangulation and quadric-based surface simplification *Comput. Geom.-Theor. Appl.* **14** 49–65

Held K, Kops E R, Krause B J, Wells W M, Kikinis R and Muller-Gartner H W 1997 Markov random field segmentation of brain MR images *IEEE Trans. Med. Imaging* **16** 878–86

Huiskamp G, Vroeijenstijn M, Van Dijk R, Wieneke G and Van Huffelen A C 1999 The need for correct realistic geometry in the inverse EEG problem *IEEE Trans. Biomed. Eng.* **46** 1281–7

Joshi M, Cui J, Doolittle K, Joshi S, Essen D V, Wang L and Miller M I 1999 Brain segmentation and the generation of cortical surfaces *Neuroimage* **9** 461–76

Kass M, Witkin A and Terzopoulos D 1987 Snakes: active contour models *Int. J. Comput. Vis.* **1** 321–31

Kristeva-Feige R *et al* 1997 Reproducibility and validity of electric source localisation with high-resolution electroencephalography *Electroencephalogr. Clin. Neurophysiol.* **103** 652–60

Lo S H 1995 Automatic mesh generation over intersecting surfaces *Int. J. Numer. Methods Eng.* **38** 943–54

Lohner R and Parikh P 1988 Generation of three-dimensional unstructured grids by the advancing-front method *Int. J. Numer. Methods Fluids* **8** 1135–49

Lorensen W E and Cline H E 1987 Marching Cubes: a high resolution 3D surface construction algorithm *Comput. Graphics* **21** 163–9

Lynn M S and Timlake W P 1968 The use of multiple deflations in the numerical solution of singular systems of equations, with applications to potential theory *SIAM J. Numer. Anal.* **5** 303–22

Meijs J, Weier O, Peters M J and Van Oosterom A 1989 On the numerical accuracy of the boundary element method *IEEE Trans. Biomed. Eng.* **36** 1038–49

Michel C M, Thut G, Morand S, Khateb A, Pegna A J, de Peralta R G, Gonzales S, Seeck M and Landis T 2001 Electric source imaging of human brain functions *Brain Res. Rev.* **36** 108–18

Nixon J B, Rasser P E, Teubner M D, Clark C R and Bottema M J 2003 Numerical model of electrical potential within the human head *Int. J. Numer. Methods Eng.* **56** 2353–66

Nobuyuki O 1979 A threshold selection method from gray-level histograms *IEEE Trans. Syst. Man Cybern.* **9** 62–6

Oostenveld R and Oostendorp T F 2002 Validating the boundary element method for forward and inverse EEG computations in the presence of a hole in the skull *Human Brain Mapp.* **17** 179–92

Özdemir M K and Gençer N G 1997 A new finite element method formulation for the forward problem solution of electro-magnetic source localization *19th Annu. Int. Conf. of the IEEE EMBS* pp 2104–7

Poston T, Wong T and Heng P 1998 Multiresolution isosurface extraction with adaptive skeleton climbing *Proc. Eurographics '98* vol 17

Rao L, He R, Li Y, Liu S and Yan W 2000 Computations of electroencephalography and magnetoencephalography for real head model *IEEE Trans. Magn.* **36** 1812–6

Riera J J and Fuentes M E 1998 Electric lead field for a piecewise homogeneous volume conductor model of the head *IEEE Trans. Biomed. Eng.* **45** 746–53

Roth B J, Balish M, Gorbach A and Sato S 1993 How well does a three-sphere model predict positions of dipoles in a realistically shaped head? *Electroencephalogr. Clin. Neurophysiol.* **87** 175–84

Rush S and Driscoll D A 1969 EEG electrode sensitivity—an application of reciprocity *IEEE Trans. Biomed. Eng.* **16** 15–22

Sandor S and Leahy R 1997 Surface-based labelling of cortical anatomy using a deformable atlas *IEEE Trans. Med. Imag.* **16** 41–54

Schimpf P, Haueisen J, Ramon C and Hannes N 1998 Realistic computer modelling of electric and magnetic fields of human head and torso *Parallel Comput.* **24** 1433–60

Shan Z Y, Yue G H and Liu J Z 2002 Automated histogram-based brain segmentation in T_1-weighted three-dimensional magnetic resonance head images *Neuroimage* **17** 1587–98

Tang H, Wu E X, Ma Q Y, Gallagher D, Perera G M and Zhuang T 2000 MRI brain image segmentation by multi-resolution edge detection and region selection *Comput. Med. Imaging Graphics* **24** 349–57

Taubin G 1995 A signal processing approach to fair surface design *Proc. of Siggraph* pp 351–8

Thevenet M, Bertrand O, Perrin F, Dumont T and Pernier J 1991 The finite element method for a realistic head model of electrical brain activities: preliminary results *Clin. Phys. Physiol. Meas.* A **12** 89–94

Vanrumste B, Van Hoey G, Van de Walle R, D'Have M R P, Lemahieu I A and Boon P A J M 2001 The validation of the finite difference method and reciprocity for solving the inverse problem in EEG dipole source analysis *Brain Topogr.* **14** 83–92

Van't Ent D, De Munck J C and Kaas A L 2001 A fast method to derive realistic BEM models for E/MEG source reconstruction *IEEE Trans. Biomed. Eng.* **48** 1434–43

Wang Y and Gotman J 2001 The influence of electrode location errors on EEG dipole source localization with a realistic head model *Clin. Neurophysiol.* **112** 1777–80

Wells W M, Grimson W E L, Kikinis R and Jolesz F A 1994 Statistical intensity correction of MRI data *Proc. SPIE* **2359** 13–24

Xu C and Prince J L 1998 Snakes, shapes and gradient vector flow *IEEE Trans. Image Process.* **7** 359–69

Yan Y, Nunez P L and Hart R T 1991 Finite-element model of the human head: scalp potentials due to dipole sources *Med. Biol. Eng. Comput.* **29** 475–81

Yvert B, Bertrand O, Echallier J F and Pernier J 1995 Improved forward EEG calculations using local mesh refinement of realistic head geometries *Electroencephalogr. Clin. Neurophysiol.* **95** 381–92

Yvert B, Crouzeix-Cheylus A and Pernier J 2001 Fast realistic modeling in bioelectromagnetism using lead-field interpolation *Human Brain Mapp.* **14** 48–63